Physica E 127 (2021) 114536

Contents lists available at ScienceDirect

Physica E: Low-dimensional Systems and Nanostructures

journal homepage: http://www.elsevier.com/locate/physe

Heat flow enhancement in a nanoscale plasmonic junction induced by Kondo resonances and electron-phonon coupling

Ali Goker [a], Huseyin Aksu [b,*], Barry D. Dunietz [c]

[a] Department of Physics, Bilecik University, 11210, Gülümbe, Bilecik, Turkey
[b] Department of Physics, Canakkale Onsekiz Mart University, 17100, Canakkale, Turkey[1]
[c] Department of Chemistry, Kent State University, Ohio, 44242, Kent, United States

ARTICLE INFO

Keywords:
Heat transport
Kondo temperature
NEGF
Plasmonic
Electron-phonon

ABSTRACT

Recently, we showed that plasmon-exciton coupling can increase entropy current through a bridge coupled to plasmonic metal nanoparticles. Here we show that electron-phonon coupling can also be used to control the entropy current in similar systems. Entropy current tends to decrease due to electron-phonon coupling and to exhibit a monotonous decrease upon temperature ramping. However, an anomaly affecting the current where it is enhanced by electron-phonon coupling is indicated at around 42 times the system's Kondo temperature. We therefore report means to control heat flow by tuning the Kondo resonance through the electron-phonon coupling. We analyze the conditions that bring about these trends due to electron-phonon coupling by employing non-equilibrium Green's function formulation addressing the entropy current and the derived heat flow.

1. Introduction

Advances in nanotechnology device fabrication over the last decades have reached in the size scale the diffraction limit of the incident radiation. A feat that bears potential to transform optoelectronic applications [1–4]. The decrease of the size scale of operational devices below the wavelength of the incident radiation achieves photo induced plasmonic resonances. This progress stands on the tunability of the plasmonic resonances in noble metal nanoparticles to focus the illumination into regions smaller than the wavelength of light [5,6].

Plasmons can be also used to improve the efficiency in photovoltaic devices primarily by directly increasing the cross section of the solar spectrum absorption [7–9], where the extinction coefficient of plasmonic metal nanoparticles is orders of magnitude larger than alternative quantum dots or dyes [10]. The absorbed energy can be efficiently transported in the form of charge carrier resulting from strong dipole-dipole coupling [11,12]. However, so far the plasmon-enhanced resonant energy transfer remains ineffective due to the short lifetime of the plasmon, in contrast to electron-hole pairs generated in a dye or quantum dot [13]. On the other hand, plasmons can form a Bose-Einstein condensate in a lattice [14], which contributes to their stability in room temperature applications.

Another potential benefit of plasmons for photovoltaic technology is by improving the control of heat transfer. Energy loss through heat remains a fundamental challenge for optimizing the efficiency of solar energy conversion. Heat transfer can be controlled by chemical means [15] or physical tuning [16]. Heat transfer and current in molecular junctions affected by electron scattering due to electron-phonon coupling are widely studied [17–23]. Heat transfer in plasmonic systems is expected to be dominated by phonons [15,16,24]. A recent computational study showed that heat transfer that decreases upon electron-phonon coupling can be further inhibited under voltage bias [25]. Similarly, decrease in heat transfer due to electron phonon coupling was shown in oligoynes molecules that bridge two gold electrodes [26].

The plasmon resonances of nanoparticles can be tuned to improve the control of heat transfer through a relatively new explored regime of strong coupling with excitons. In such a scenario, the plasmonic resonances induce large electromagnetic field [27,28] that interacts strongly with nearby quantum emitters. The resulting strong coupling of plasmons with the resonant excitations of the quantum emitter gives rise to light-matter modes that are called plexcitons. These intriguing hybrid light-matter modes, that present a relative new field of explored physics, are well delocalized across the nanoparticle and open the door to design

* Corresponding author.
E-mail addresses: aihsan.goker@bilecik.edu.tr (A. Goker), haksu@kent.edu (H. Aksu).
[1] Department of Chemistry, Kent State University, Ohio 44242, Kent, United States.

https://doi.org/10.1016/j.physe.2020.114536
Received 22 August 2020; Received in revised form 1 November 2020; Accepted 12 November 2020
Available online 26 November 2020

means for the control of energy loss in the form of heat. Indeed, the design of devices to include plexcitons bears enormous potential to improve the efficiency in various applications including those of opto-electronic devices [29], lasing [30] and photocatalysis [31].

There have been several theoretical studies on plexcitons in nano-junctions based on classical transformation optics [32], a semiclassical electrostatic eigenmode model [33] and a hybrid technique that merges a discrete interaction model with quantum mechanics [34]. A relevant quantum mechanical model that allows to account well for the contribution of the spin degrees of freedom within the quantum emitter can be achieved using Green's function (GF) formulation [35]. For example, relevant studies using this approach identified the dipolar plasmon mode as means to control the current in systems affected by strong plasmon-exciton coupling. In addition calculations based on GF approach with the non-crossing approximation (NCA) achieved the first analysis of the interplay between the strong electron correlations within the quantum emitter and the plexcitons [36]. This work highlighted the crucial role of electron correlations, relating the Fano resonances in the optical emission spectrum to plasmon-exciton coupling. The same technique was later used to investigate the role of strong electron correlation in the electrical conductance [37], which is enhanced with the increase of plasmon-exciton coupling at ambient temperatures around or below the Kondo temperature. Similarly, the entropy current, for a Coulomb blockaded quantum emitter bearing strong onsite electron correlation increases with plasmon-exciton coupling [38]. Nevertheless, a realistic picture of plexcitons and their effect on heat current has not emerged yet. In particular, to the best of our knowledge none of the earlier studies addressed the role of electron-phonon coupling within the quantum emitter which are expected to play an important role in affecting the response of the heat flow to plexitons.

In this paper, we report control of heat flow by tuning electron-phonon coupling in junctions affected by Kondo resonances. The temperature dependence of the entropy current through a plexcitonic nanojunction is analyzed, where we address directly the effects of vibration and strong electron correlation within the quantum emitter. We implement a sophisticated many-body theory on a relatively simple model to study the generation of plexitons in plasmonic nanojunctions. We address means to control the heat transfer based on induced Kondo resonances by tuning electron-phonon coupling.

2. Computational approach

2.1. Model

The nanojunction consists of a quantum emitter bridging two metal nanoparticles shown schematically in Fig. 1. Two spin degenerate levels within the quantum emitter are designated by $|g\rangle$ and $|e\rangle$ with an energy gap of $|\epsilon_e - \epsilon_g|$. The emitter states are coupled to the nanoparticles through the plasmon-exciton coupling Δ_K, where K corresponds to L or R nanoparticles. The plasmonic nanoparticles are excited by laser radiation, while the nanojunction is affected by an infitismal voltage bias and a temperature gradient across the nanoparticles of T_L to T_R.

For each emitter level, s, $c^\dagger_{s\sigma}(c_{s\sigma})$ creates (annihilates) an electron with spin σ, and for the metal nanoparticle plasmonic states we note the creator (annihilator) operator as $c^\dagger_{K\sigma}(c_{K\sigma})$. Similarly, $b^\dagger_K(b_K)$ is the bosonic operators that creates (annihilates) a plasmon of energy ϵ_{pK} in the nanoparticle. The laser frequency is represented by the energy parameter ϵ_α. J is the amplitude of the electron transfer integral between $|g\rangle$ and $|e\rangle$, $V_{K,g(e)}$ denotes the coupling amplitude between the metal nanoparticle, K, and $|g(e)\rangle$. $W_{\alpha,K}$ represents the interaction strength between the laser irradiation in mode α and the dipolar plasmon modes of each nanoparticle. Δ_K corresponds to the strength of the coupling between the dipolar plasmon modes of the left or right metal nanoparticle and the exciton formed in the quantum emitter. Finally, λ denotes the strength of the electron-phonon coupling with $d^\dagger(d)$ creating

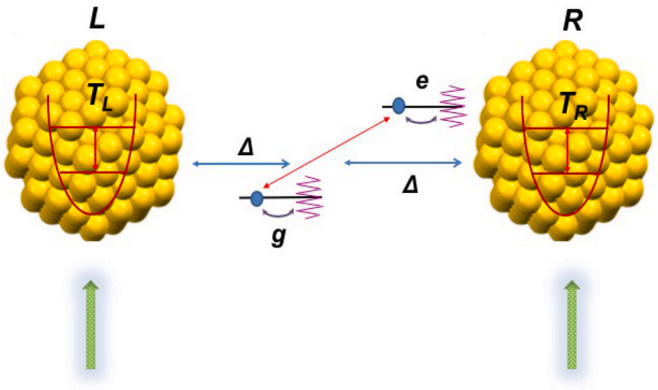

Fig. 1. A nanojunction made up of a two level quantum emitter, $|g\rangle$ and e, located between two plasmonic metal nanoparticles at T_L and T_R temperatures. The junction is affected by a sufficient large voltage bias and temperature difference. The laser radiation excites plasmon modes of the nanoparticles, leads to the electronic excitation energy through plasmon-exciton coupling, Δ. The electron-phonon coupling, λ, is indicated by the purple lines. (For interpretation of the references to colour in this figure legend, the reader is referred to the Web version of this article.)

(annihilating) a phonon localized within the quantum emitter and ω_0 is the phonon energy.

The Hamiltonian representing this nanojunction addressing the emitter states and plasmons includes the following terms:

$$H = H_N + H_{EN} + \sum_{\alpha\in\{E,\mathrm{rad}\}} (H_\alpha + V_\alpha). \tag{1}$$

The H_N term represents the metal nanoparticles such that

$$H_N = \sum_{K\in\{L,R\},\sigma} \epsilon_{K\sigma} c^\dagger_{K\sigma} c_{K\sigma} + \sum_{K\in\{L,R\}} \epsilon_{pK} b^\dagger_K b_K, \tag{2}$$

The H_{EN} terms introduce the plasmon-exciton coupling

$$H_{EN} = \sum_{K\in\{L,R\},\sigma} \left(\Delta_K c^\dagger_{e\sigma} c_{g\sigma} b_K + h.c.\right) \tag{3}$$

The H_E terms address the quantum emitter states

$$\begin{aligned} H_E &= \sum_{s\in\{g,e\},\sigma} [\epsilon_s + \lambda(d + d^\dagger)] c^\dagger_{s\sigma} c_{s\sigma} + \omega_0 d^\dagger d \\ &\quad + J\sum_\sigma \left(c^\dagger_{g\sigma} c_{e\sigma} + h.c.\right) + \frac{U}{2} \sum_{s\in\{g,e\}} n_{s\sigma} n_{s\sigma'}, \end{aligned} \tag{4}$$

and V_E coupling of the emitter states to the electronic states in the metal nanoparticles

$$V_E = \sum_{K\in\{L,R\},\sigma} \left(V_{K,g(e)} c^\dagger_{K\sigma} c_{g(e)\sigma} + h.c.\right) \tag{5}$$

The electronic tunneling that couples the metal nanoparticles and the quantum emitter states $\overline{\Gamma}$ is defined as follows:

$$\begin{aligned} \overline{\Gamma} &= \overline{\Gamma}_{L,g} = 2\pi |V_{L,g}(\epsilon_f)|^2 \\ \overline{\Gamma} &= \overline{\Gamma}_{R,e} = 2\pi |V_{R,e}(\epsilon_f)|^2, \end{aligned} \tag{6}$$

where Γ is defined as $\Gamma \equiv \overline{\Gamma}\rho(\epsilon_f)$, and $\rho(\epsilon_f)$ is the density of states of the metal nanoparticles at the Fermi level. Importantly below we consider the regime of strong electron-phonon coupling, λ, that is comparable to the electronic coupling, Γ.

A canonical transformation can be used to drop the strong electron-phonon coupling term. Here we use the unitary Lang-Firsov canonical transformation [39].

$$S = \exp\left[\frac{\lambda}{\omega_0}\sum_{s,\sigma} c_{s\sigma}^{\dagger}c_{s\sigma}(d^{\dagger}-d)\right] \tag{7}$$

The outcome of this transformation is

$$\begin{aligned} SdS^{\dagger} &= d - \frac{\lambda}{\omega_0}\sum_{s,\sigma} c_{s\sigma}^{\dagger}c_{s\sigma} \\ Sc_{s\sigma}S^{\dagger} &= c_{s\sigma}X, \end{aligned} \tag{8}$$

where

$$X = \exp\left[-\frac{\lambda}{\omega_0}(d^{\dagger}-d)\right] \tag{9}$$

The electron operators in the quantum emitter acquire X after this transformation, which indicates polaron formation at the junction.

This transformation converts the Hamiltonian describing the quantum emitter into

$$\begin{aligned} \overline{H}_E = SH_ES^{\dagger} = \sum_{s\in\{g,e\},\sigma}\left(\epsilon_s - \frac{\lambda^2}{\omega_0}\right)c_{s\sigma}^{\dagger}c_{s\sigma} + \omega_0 d^{\dagger}d + \\ J\sum_{\sigma}\left(c_{g\sigma}^{\dagger}c_{e\sigma} + h.c.\right) + \left(\frac{U}{2} - \frac{2\lambda^2}{\omega_0}\right)\sum_{s\in\{g,e\}} n_{s\sigma}n_{s\sigma'}, \end{aligned} \tag{10}$$

which results in renormalization of the discrete levels and the Hubbard interaction as $\overline{\epsilon}_s = \epsilon_s - \lambda^2/\omega_0$ and $\overline{U} = U/2 - (2\lambda^2/\omega_0)$ respectively. The electronic population distribution depends on the discrete levels. Therefore, the inelastic effects directly alter the electronic population in discrete states due to the renormalization.

Despite the renormalization of the Hubbard interaction strength, it is still much larger than the linewidth of each discrete level owing to the close confinement of electrons. Therefore, this amounts to $\overline{U}\to\infty$ for all practical purposes. This essentially restricts the occupancy of each discrete level to a single electron. In order to be able to apply standard diagrammatic techniques to this case, the original electron operators are written in terms of a massless boson (b) and a pseudofermion operator (f) as

$$\begin{aligned} c_{g(e)\sigma} &= b_{g(e)}^{\dagger}f_{g(e)\sigma} \\ c_{g(e)\sigma}^{\dagger} &= f_{g(e)\sigma}^{\dagger}b_{g(e)}, \end{aligned} \tag{11}$$

provided that

$$Q_{B,g(e)} = b_{g(e)}^{\dagger}b_{g(e)} + \sum_{\sigma} f_{g(e)\sigma}^{\dagger}f_{g(e)\sigma} = 1. \tag{12}$$

This boson operator keeps the occupancy of each discrete level to unity while allowing to discard the Hubbard term from the Hamiltonian altogether. Consequently, the Hamiltonian term that models the quantum emitter is reduced to

$$\begin{aligned} \overline{H}_E = \sum_{s\in\{g,e\},\sigma}\overline{\epsilon}_s f_{s\sigma}^{\dagger}f_{s\sigma} + \omega_0 d^{\dagger}d + \\ J\sum_{\sigma}\left(f_{g\sigma}^{\dagger}f_{e\sigma} + h.c.\right), \end{aligned} \tag{13}$$

while the tunneling Hamiltonian becomes

$$\overline{V}_E = \sum_{K\in\{L,R\},\sigma}\left(\widetilde{V}_{K,g(e)}c_{K\sigma}^{\dagger}b_{g(e)}^{\dagger}f_{g(e)\sigma} + h.c.\right) \tag{14}$$

with

$$\widetilde{V}_{K,g(e)} = V_{K,g(e)}\exp\ -V_{e-p}(N_{ph} + 1/2), \tag{15}$$

In the last equation we consider the expectation value of the phonon operator. This expression of the operator is valid only when the hopping is small compared to the electron-phonon interaction, i.e. $V_{K,g(e)} \ll \lambda$ [40] a condition that is satisfied by the paramaters used below. The replacement of the phonon operator with its expectation value in this formalism assumes the formation of a polaron in the junction [41].

In Eq. (15), $V_{e-p} = (\lambda/\omega_0)^2$ will be referred to as the electron-phonon coupling strength from now on and N_{ph} stands for the number of phonons, which obeys the usual Bose-Einstein statistics at any given temperature T. We note that the above equations converge to the approach adopted in our previous study [38] only in the limit where $\lambda \to 0$. The last term adds the interaction due to quantum emitter and the radiation. The laser radiation is included via

$$H_{\mathrm{rad}} = \sum_{\alpha}\epsilon_{\alpha}a_{\alpha}^{\dagger}a_{\alpha} \tag{16}$$

while V_{rad} corresponds to the interaction between the laser radiation and the plasmon modes of each nanoparticle

$$V_{\mathrm{rad}} = \sum_{K\in\{L,R\},\alpha}\left(W_{\alpha,K}a_{\alpha}^{\dagger}b_K + h.c.\right) \tag{17}$$

2.2. Model setup

The discrete levels in the quantum emitter are placed at $\epsilon_g = -4.8$ eV and $\epsilon_e = -1.6$ eV. Here, the minus sign indicates that the levels lie below the Fermi level of the metal nanoparticles ϵ_f which is set to zero reference energy. To enforce Coloumb blockade we set $U \to \infty$, so that current flows only when the Kondo resonance exists. The dipolar plasmon energy $\epsilon_p = 3.49$ eV, the laser bandwidth $\delta = 1$ meV and the laser coupling to the dipolar plasmon mode $\gamma = 2\pi|W_0|^2 = 86$ meV. These values are the same as used in earlier studies and allow to highlight the effect of electron-phonon coupling that were not included in those studies [36–38,42].

The two nanoparticles are associated with the same parabolic density of states with half bandwidth of $D = 7.2$ eV. The left nanoparticle is kept at ambient temperature, i.e. $T_L = T$. For these parameters, non-renormalized $T_{K,e}$ turns out to be around 23 K while $T_{K,g} \approx 0$. This means that ϵ_g remains under Coulomb blockade for any experimentally relevant temperature. In the rest of the discussion we drop the state subscript in referring to the Kondo temperature of either nanoparticle by addressing to $|e\rangle$, since $T_{K,g}$ is effectively zero on the absolute scale. We set $\omega_0 = 0.06\Gamma$ as a constant and vary λ to control the electron-phonon coupling $V_{e-p} = \lambda^2/\omega_0^2$. The strength of the electron-phonon coupling, λ, is established by comparing to the electronic coupling, Γ. Here we study $\lambda = 0.09\Gamma$ and $\lambda = 0.116\Gamma$, where the electron-coupling is significant enough to justify a canonical transformation, while not strong enough to quench the Kondo resonance entirely [43].

There are two characteristic timescales governing the dynamics of this system. The timescale for the electron transfer is $\tau_e = 1/T_{K,e}$, and the timescale for the phonons is $\tau_p = 1/\omega_0$, where τ_e is an order of magnitude larger than τ_p. This is physically reasonable since the electron transfer is expected to occur only once the Kondo resonance is developed and it takes quite a considerable time for the Kondo resonance to build up as shown in Ref. 40 [44].

A single mode laser with energy ϵ_0 is assumed to pump only the dipolar plasmon mode of the metal nanoparticles where excitations of the quantum emitter by the laser beam is ignored. This enables to drop the J term in H_E. It is then permitted to set the dipolar plasmon energy for each nanoparticle to $\epsilon_{pL} = \epsilon_{pR} = \epsilon_p$ in conjunction with considering symmetrical plasmon-exciton and plasmon-laser couplings $\Delta_L = \Delta_R = \Delta$ and $W_{0,L} = W_{0,R} = W_0$. Finally, to tune the effective non-equilibrium condition of a temprature gradient either the intensity of the laser beam can be adjusted, or the plasmonic states of the nanoparticles can be varied to represent different sizes.

2.3. Quantum transport modeling

We now turn to describe the quantum transport corresponding to the model depicted above and in particular address the Kondo resonance. Non-equilibrium GFs expressions in the two time variables space are adopted to investigate the dynamical quantum transport. We refer to the Appendix and references for the definitions of the GFs in terms of the operators introduced above and for detailed descriptions of the Dyson equations and the numerical solution procedure [36,45,46].

The discrete energy levels $|g\rangle$ and $|e\rangle$ of the quantum emitter are not directly coupled, where each is coupled to only one of the plasmonic nanoparticles leading to a blockade. However, a laser excitation of the metal nanoparticles and plasmon-exciton coupling enable transition between the excitonic emitter states ($|g\rangle$ to $|e\rangle$). The mechanism that overcomes the blockade relies on a many body state forming the Kondo resonance. Accordingly, an electron in $|e\rangle$ tunnels to the right nanoparticle essentially lifting the blockade, where an electron with an opposite spin in $|g\rangle$ tunnels through the plasmon-exciton coupling to the now vacant $|e\rangle$ almost simultaneously. This is equivalent to a spin flip at the particular energy level [47], which induces current flow inspite of the Coulomb blockade. In order to form a Kondo resonance, electrons must tunnel almost simultaneously. This amount to a cotunneling process. Hence, when an electron with spin up leaves $|e>$ level, another electron with the opposite spin must replace it so that the antiferromagnetic interaction between the spins of two electrons will form a spin singlet with orbital angular momentum $L = 0$. This is the main requirement for the development of the Kondo resonance. Unless the Kondo resonance develops, the system will remain in Coulomb blockade and the transport will be blocked. Therefore, an electron with the same spin cannot occupy $|e>$ in a Coulomb blockaded system once it is vacated. This can be possible only in a tight binding model which is not our configuration in this paper. Spin flip processes involving a single level exist. Nevertheless, these processes do not affect the transport between the left and right metal nanoparticles. We only describe the processes that contribute to the heat flow between the left and right nanoparticles..

The formation of Kondo resonance requires positioning the emitter state energies below the Fermi level of the metal nanoparticles ϵ_f. The sharp Kondo resonance builds up in the density of states (DOS) slightly above ϵ_f and is maximized at or below the Kondo temperature [48]. The corresponding Kondo temperature depends on the nanoparticles' DOS, the emitter state energy ϵ_g, and the electronic coupling Γ, as follows:

$$T_{K,g} \simeq \left(\frac{D\Gamma}{4}\right)^{\frac{1}{2}} \exp\left(-\frac{\pi|\epsilon_g|}{\Gamma}\right) \tag{18}$$

In this expression, D is the half bandwidth of the density of states of the metal nanoparticles. Since the energy gap $|\epsilon_e - \epsilon_g|$ in our model is very large, the problem can still be effectively treated as SU(2) symmetry [49].

The replacement of the phonon operator with its expectation value predicts that the Kondo temperature changes exponentially with the electron-phonon coupling, but it has been claimed not to be true [50,51]. There are also previous works which incorporated the phonons within the NCA without this decoupling [52,53]. The latter work has some similarity with ours because it has two levels hybridized with conducting leads and phonons, and discusses the Kondo temperature T_K. Nevertheless, we conclude that our results are still valid, even though the renormalized value of T_K is probably somewhat underestimated. This issue does not effect our calculations because we do not claim to know the precise renormalized value of T_K and all our graphs are plotted in terms of T/T_K where T_K is the non-renormalized value (i.e. in the absence of electron-phonon coupling). Furthermore, the value of T_K is not an input to our calculations whether it is renormalized or not.We just use its reduction in the presence of finite electron-phonon coupling as a benchmark to interpret our results. Hence, this pathological situation does not invalidate our results in any way.

An approximation is needed to tackle the strong electron correlations that arise in the limit $u \to \infty$. We resort to the well-established NCA [44,45] to write the self-energies of pseudofermions and slave bosons introduced above in eq. (11). (The detailed expressions of the affected pseudofermion and slaveboson self-energies in the Dyson equations are detailed in the appendix.) NCA was applied to study electrical conductance of a single quantum dot coupled to metallic electrodes [54], where the experimental values above $0.1T_K$ were reproduced well. Furthermore, NCA was found to capture the Kondo resonance in the density of states quite accurately at ambient temperatures well below T_K [48,55]. In general, NCA was found to estimate reliably physical observables even at low ambient temperatures T, provided that $T > T_p$, where $T_p/T_K \approx \pi T_K/\Gamma$ [56]. At the lower temperatures, $T < T_p$, the NCA fails to reproduce experimental results due to the departure from the Fermi liquid behaviour [56]. Below we find that $T_p \approx 0.18$ K ($T_K = 23$ K and $\Gamma = 0.8$ eV) validating the use of the NCA at temperatures above this low limit.

The entropy current through this nanojunction, from which heat flow can be directly be deduced, is defined in terms of the energy (I^E) and particle currents (I) as [38].

$$I^s = \frac{I^E_L - \mu_L I_L}{T_L} + \frac{I^E_R - \mu_R I_R}{T_R} + \frac{I^E_\gamma - \mu_\gamma I_\gamma}{T_\gamma}, \tag{19}$$

where the nominator in each term corresponds to the decomposition of the heat current, which can be expressed as $I_h = KA\Delta T$. Here, ΔT is the temperature gradient, A is the cross section of the junction and K is the thermal conductivity. Therefore, the entropy current can be directly contrasted to measured heat flow at a specific temperature [57,58]. In Eq. (19), the first two terms correspond to the left (L) and right (R) electron reservoirs, whereas the third term represents the photon bath (γ). We assume no direct coupling between the photon bath and the quantum emitter, thus the contribution of the photon bath to the entropy current is captured by the plasmon Green functions. See the Appendix for more information.

The radiation field current is given by

$$\begin{aligned} I^E_{\gamma,g(e)}(t) = Re \int_{-\infty}^{t} dt_1 \Big(- \Big(g_{g(e)}(t,t_1) B^<_{g(e)}(t_1,t) \\ + G^<_{g(e)}(t,t_1) e^{\varphi(t-t_1)} b_{g(e)}(t_1,t) \Big) \Xi^<_\gamma(t_1,t) - i \Big(G^<_{g(e)}(t,t_1) e^{\varphi(t-t_1)} \\ b_{g(e)}(t_1,t) \Big) \Xi^a_\gamma(t_1,t) \Big) \Big) \end{aligned} \tag{20}$$

This is a general expression of the current assuming the coupling of the electrons within the quantum emitter with an external bosonic bath adapted to the auxiliary particle formalism. Here, $\Xi^{>(<)}_\gamma(t_1,t)$ corresponds to the self-energy of the photons due to the coupling to the quantum emitter. Since there is no direct coupling of the radiation field to the quantum emitter, the contribution of this term to the entropy current vanishes. Nevertheless, the radiation field contributes indirectly through the excitation of the plasmon modes in the metal nanoparticles. These plasmon modes interact with the quantum emitter via the plasmon-exciton coupling.

The lesser Green functions can be defined in connection with the operators introduced as $\overline{G}^<_{g(e)}(t,t') = G^<_{g(e)}(t,t') e^{\varphi(t-t')} = < f^\dagger_{g(e)\sigma}(t') f_{g(e)\sigma}(t) > e^{\varphi(t-t')}$ and $B^<_{g(e)}(t,t') = < b^\dagger_{g(e)}(t') b_{g(e)}(t) >$ while the greater ones are $\overline{G}^>_{g(e)}(t,t') = G^>_{g(e)}(t,t') e^{\varphi(t'-t)} = < f_{g(e)\sigma}(t) f^\dagger_{g(e)\sigma}(t') > e^{\varphi(t'-t)}$ and $B^>_{g(e)}(t,t') = < b_{g(e)}(t) b^\dagger_{g(e)}(t') >$. In these expressions, phase factors defined as $\varphi(t-t') = \log_e < X^\dagger(t') X(t) >$ turn out to be [43].

$$\begin{aligned} \varphi(t-t') = & -V_{e-p} N_{ph} (1 - e^{-i\omega_0(t-t')}) - \\ & V_{e-p}(N_{ph}+1)(1 - e^{i\omega_0(t-t')}), \end{aligned} \tag{21}$$

where $V_{e-p} = \lambda^2/\omega_0^2$. The combination of these analytic pieces yields the

retarded functions such that

$$\begin{aligned} G^r_{g(e)}(t,t') &= -i\theta(t-t')[G^>_{g(e)}(t,t')e^{\varphi(t'-t)} + \\ &\quad G^<_{g(e)}(t,t')e^{\varphi(t-t')}] \\ &= -i\theta(t-t')g_{g(e)}(t,t') \\ B^r_{g(e)}(t,t') &= -i\theta(t-t')[B^>_{g(e)}(t,t') - B^<_{g(e)}(t,t')] \\ &= -i\theta(t-t')b_{g(e)}(t,t'). \end{aligned} \tag{22}$$

Since the left and right nanoparticles are assumed to be coupled only to $|g\rangle$ and $|e\rangle$ respectively, the non-vanishing components of the particle current can be cast in terms of the Green functions as

$$\begin{aligned} I_{Lg}(t) &= -2\overline{\Gamma}Re\int_{-\infty}^{t} dt_1 G^<_g(t,t_1)e^{\varphi(t-t_1)}b_g(t_1,t)h(t-t_1) \\ &+2\overline{\Gamma}Re\int_{-\infty}^{t} dt_1 (g_g(t,t_1)B^<_g(t_1,t) + G^<_g(t,t_1)e^{\varphi(t-t_1)} \\ &\quad b_g(t_1,t))f_L(t-t_1) \end{aligned} \tag{23}$$

and

$$\begin{aligned} I_{Re}(t) &= -2\overline{\Gamma}Re\int_{-\infty}^{t} dt_1 G^<_e(t,t_1)e^{\varphi(t-t_1)}b_e(t_1,t)h(t-t_1) \\ &+2\overline{\Gamma}Re\int_{-\infty}^{t} dt_1 (g_e(t,t_1)B^<_e(t_1,t) + G^<_e(t,t_1)e^{\varphi(t-t_1)} \\ &\quad b_e(t_1,t))f_R(t-t_1). \end{aligned} \tag{24}$$

In these expressions

$$h(t-t_1) = \int_{-D}^{D}\frac{d\epsilon}{2\pi}\rho(\epsilon)e^{i\epsilon(t-t_1)}, \tag{25}$$

$$f_L(t-t_1) = \int_{-D}^{D}\frac{d\epsilon}{2\pi}\rho(\epsilon)\frac{e^{i\epsilon(t-t_1)}}{1+e^{\beta_L(\epsilon-V/2)}} \tag{26}$$

and

$$f_R(t-t_1) = \int_{-D}^{D}\frac{d\epsilon}{2\pi}\rho(\epsilon)\frac{e^{i\epsilon(t-t_1)}}{1+e^{\beta_R(\epsilon+V/2)}}. \tag{27}$$

Concurrently, the energy currents flowing through $|g\rangle$ and $|e\rangle$ between the left and right nanoparticles are given by

$$\begin{aligned} I^E_{Lg}(t) &= -2\overline{\Gamma}Re\int_{-\infty}^{t} dt_1 G^<_g(t,t_1)e^{\varphi(t-t_1)}b_g(t_1,t)h^E(t-t_1) \\ &+2\overline{\Gamma}Re\int_{-\infty}^{t} dt_1 (g_g(t,t_1)B^<_g(t_1,t) + G^<_g(t,t_1)e^{\varphi(t-t_1)} \\ &\quad b_g(t_1,t))f^E_L(t-t_1) \end{aligned} \tag{28}$$

and

$$\begin{aligned} I^E_{Re}(t) &= -2\overline{\Gamma}Re\int_{-\infty}^{t} dt_1 G^<_e(t,t_1)e^{\varphi(t-t_1)}b_e(t_1,t)h^E(t-t_1) \\ &+2\overline{\Gamma}Re\int_{-\infty}^{t} dt_1 (g_e(t,t_1)B^<_e(t_1,t) + G^<_e(t,t_1)e^{\varphi(t-t_1)} \\ &\quad b_e(t_1,t))f^E_R(t-t_1), \end{aligned} \tag{29}$$

where

$$h^E(t-t_1) = \int_{-D}^{D}\frac{d\epsilon}{2\pi}\rho(\epsilon)\epsilon e^{i\epsilon(t-t_1)}, \tag{30}$$

$$f^E_L(t-t_1) = \int_{-D}^{D}\frac{d\epsilon}{2\pi}\rho(\epsilon)\epsilon\frac{e^{i\epsilon(t-t_1)}}{1+e^{\beta_L(\epsilon-V/2)}} \tag{31}$$

and

$$f^E_R(t-t_1) = \int_{-D}^{D}\frac{d\epsilon}{2\pi}\rho(\epsilon)\epsilon\frac{e^{i\epsilon(t-t_1)}}{1+e^{\beta_R(\epsilon+V/2)}}. \tag{32}$$

In expressing the entropy current the electron-phonon coupling is affected by the phase factors between two phonon operators at different times attached to the lesser pseudofermion Green functions. This approach results from the NCA as discussed after eq. (15). In the limit of vanishing electron-phonon coupling $V_{e-p} = 0$, the phase becomes zero, recovering the previously reported formulas [38].

3. Results and discussion

We investigate the effect of electron-phonon coupling on the thermodynamics of the nanojunction composed of the emitter states suspended between the two nanoparticles. We start by considering low temperature of $0.12T_K$ under several plasmon-exciton coupling strengths, and where electron-phonon coupling is included. In particular, as shown in Fig. 2, the electron-phonon coupling affects a significant *suppression* of the current, while plasmonic-electronic coupling bears the opposite effect of enhancing the current [38]. The suppression of the entropy current due to electron-phonon coupling is observed at several values of plasmon-exciton coupling. The trends of the current to decrease with the electron-phonon coupling is indicated by the solid lines, whereas the trend of the current to increase with plasmonic coupling is indicated by the shaded lines.

We next follow the effect of the phonon coupling on the entropy current as the temperature is ramped up and again for various plasmon-exciton coupling strengths in Fig. 3. The overall effect of the increased temperature appears to reduce the entropy current [38]. (The temperature gradient is kept the same in all cases.) At sufficiently large temperatures the entropy current vanishes. See inserts included in the three panels each of the different electron plasmonic coupling values.

The current suppression originates from the energetic stabilization of the discrete energy levels $\overline{\epsilon}_{g(e)}$ as well as the weakening of the tunnel coupling in Eq. (15) due to the renormalization induced by finite electron-phonon coupling. These two effects jointly lower the Kondo temperature in Eq. (18) as both the prefactor and the exponent decrease in value with the increase of the coupling. Consequently the entropy current is further suppressed as the temperature is incremented when affected by the electron-phonon coupling. The most discernible effect of finite electron-phonon coupling is to suppress the sharp Kondo resonance appearing in the density of states at fixed ambient temperature via

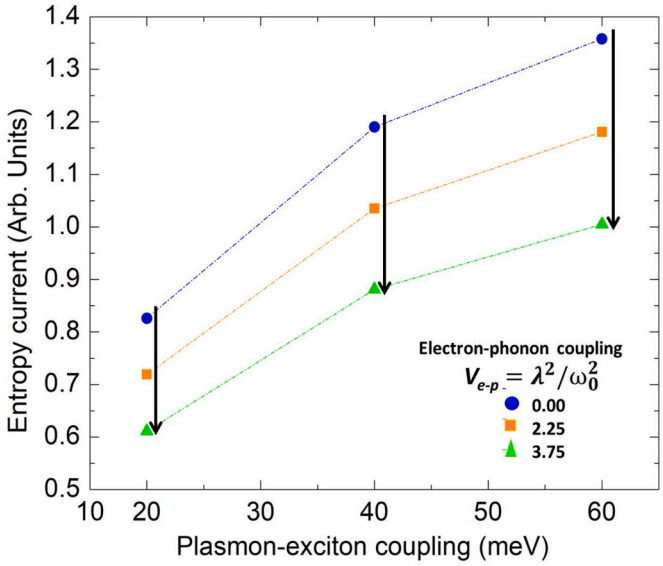

Fig. 2. The entropy current drops with the increase of electron phonon coupling shown for three cases of plasmon-exciton coupling (20, 40 and 60 meV) at low temperature of $0.12T_K$. The current increases with the plasmon-exciton coupling, see dotted lines [36].

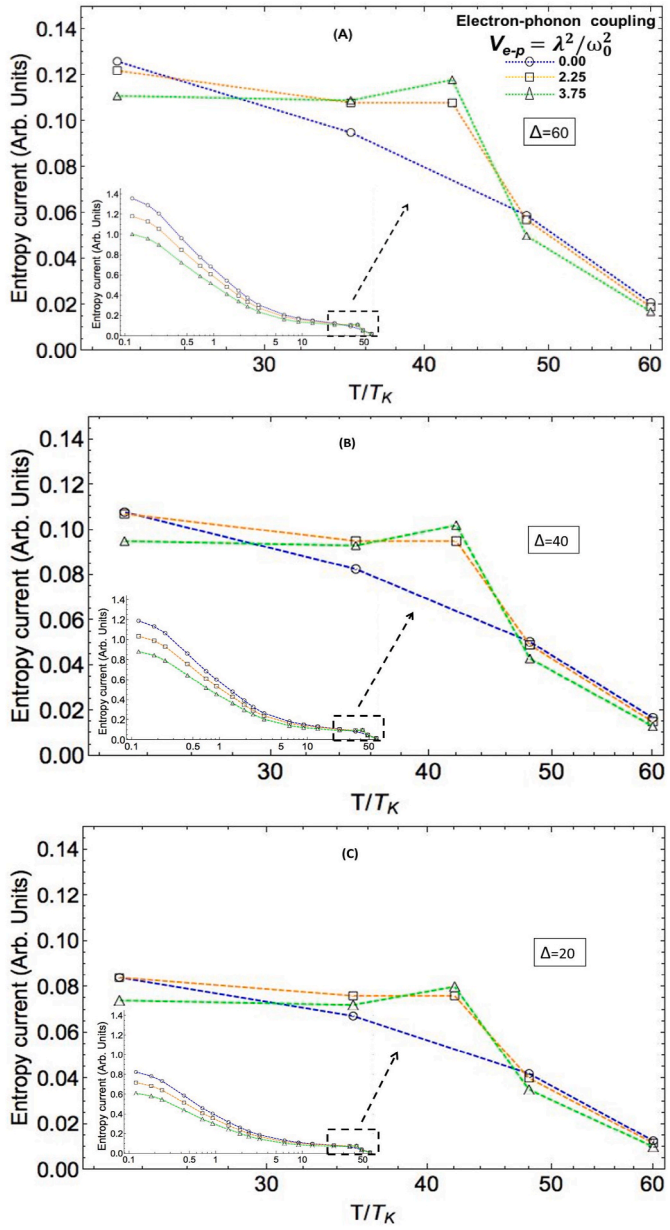

Fig. 3. Entropy current as a function of the temperature, obtained with electron-phonon coupling values $V_{e-p} = 0.00$ [43], 2.25 and 3.75. Results are shown in three panels A, B, and C corresponding to plasmon-exciton coupling strengths $\Delta = 60$, 40 and 20, respectively. The currents are obtained under infinitesimal bias and a temperature gradient of $\Delta T = 2$ K between the metal nanoparticles. An anomaly in the current at temperature of about 42 times of the Kondo temperature is indicated. The insets show the overall temperature dependence of the current.

the renormalization of T_K. Now, the Kondo resonance reaches its full prominence at ambient temperatures below T_K, thus the suppression is more pronounced in this regime than the case where the Kondo resonance is vanishingly small at $T \gg T_K$. This naturally results in a sharper drop in the entropy current values at low temperature regime versus the high temperature regime.

However, there appears to be a deviation of this trend of current decrease with the temperature. As indicated in the figure, an anomaly, where the decrease in current is suspended, is observed around $T \approx 42T_K$. This anomaly is noted for all the considered plasmon-exciton coupling strengths (see the three panels), and in fact shows an increase of the current with temperature (in a small range of temperatures). Importantly, the anomaly depends on the electron-phonon coupling as indicated by the increase of the current upon increase of the phonon coupling. The green line that corresponds to the strongest phonon coupling case is associated with the largest current at $T \approx 42T_K$, while it is the smallest in other temperatures. Indeed these complex effects of phonon coupling on the current are reflected in Fig. 4. In most temperatures the current is suppressed by phonon coupling as shown by the shaded dashed lines, whereas the trend of current increase with the coupling is observed for the blue line of $T \approx 42T_K$. The half-bandwidth of the metal nanoparticles is given as $D = 7.2$ eV and the dipolar plasmon energy is given as $\varepsilon_p = 3.49$ eV whereas $42T_K$ corresponds to 83 meV. This is roughly equal to the laser coupling to the dipolar plasmon mode which is 86 meV and much smaller than the other two energy scales mentioned above. A plot of the Lorentz number L as a function of temperature for various electron-phonon coupling strengths is given in Fig. 4 of Ref. 58. We refer the readers to consult that figure.

We address the general trend where the current is suppressed by phonon coupling, and where at a particular range of temperatures determined by the Kondo resonance the phonon coupling enhances the current. To understand these trends we express the current by [38].

$$I^s = \frac{I_R^h}{T_R} = \frac{\Delta TGLT}{T - \Delta T}. \tag{33}$$

Here G stands for the electrical conductance and L denotes the Lorentz number, which quantifies the relation between the electrical and thermal conductivities of metals for a given temperature T in Wiedemann-Franz law. It is appropriate to note here that in practice L values can deviate from the textbook value $L_0 = \frac{\pi^2 k_B^2}{3e^2}$ considerably and therefore may bear a significant effect on the measured current.

We consider first the general trend of phonon coupling to suppress the current. In the limit of infinitesimal bias, it has been shown that the nonlinear corrections to L are negligible [38]. Therefore, the temperature dependence of the entropy current shown in Fig. 3 is due to the dependence of L and the electrical conductance G. As explained above similarly to the electrical conductance that is suppressed by electron-phonon coupling [37], the entropy current tends to be suppressed by the phonon coupling.

To explain the origin of the anomaly, we follow L as affected by a further increase of the temperature in the context of Equation. As shown

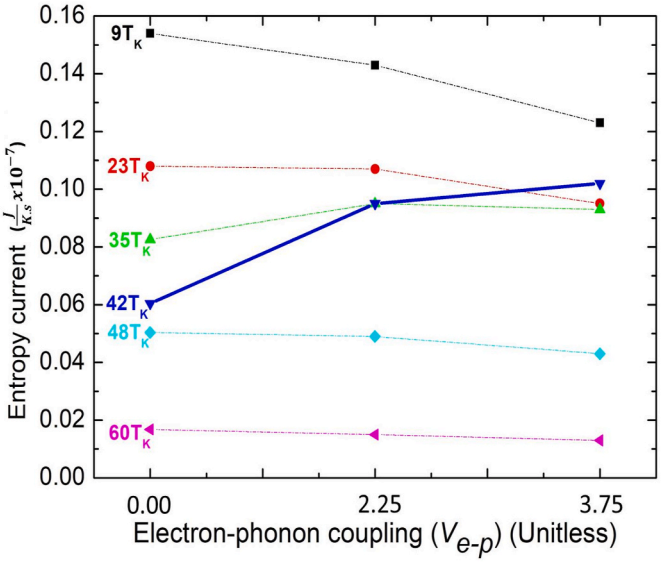

Fig. 4. The entropy current with the increase of electron phonon coupling is shown for a fixed plasmon-exciton coupling, $\Delta = 40$ meV and several ambient temperatures. The general trend of current inhibition is demostrated by the finer lines while the anomaly of current increase is indicated at $\approx 42T_K$.

previously, under a finite electron-phonon coupling effect, the L dependence on the temperature changes sign from a negative slope (for low T) to a positive slope (for high T), a transition that occurs at around $42T_K$ [59]. The L appears to become constant at the higher temperatures at the limit of vanishing coupling. Indeed under a larger enough temperature and a finite electron-phonon coupling the L collapses. Importantly at the transition temperature of about $42T_K$, the L is reaching a maximal value, resulting in the anomaly of increased heat current with the temperature.

4. Conclusions

We study the effect of electron-phonon coupling on the heat current across a nanojunction to design means to control the flow. Three models consist of a two level quantum emitter sandwiched between metal nanoparticles supporting plasmon modes. Nonequilibrium Green function formulation addressing electron dynamics is used to calculate entropy current affected by both electron phonon and electron plasmonic coupling terms. The heat flow can be directly inferred from the calculated entropy current, therefore presenting means to control the flow.

We show that entropy current is suppressed by the increase of the temperature. This trend is further enhanced by electron-phonon coupling that appears to synergize the effect of the temperature to suppress the current. Interestingly, this effect of the phonon coupling is reversed by a dynamical buildup of the Kondo resonance. The presence of phonon coupling at around $T \approx 42T_K$ the monotonous decline of the entropy current (and therefore of heat flow) by the ambient temperature is reversed, finding, instead, current increase with the temperature increase. We relate this complex effect of electron-phonon coupling on the Kondo resonance leading to dynamical response of the Lorentz number.

The relationships of phonon coupling and entropy current analyzed in this report bear potential to impact the design of state-of-the-art optoelectronic applications as means for controlling the heat flow. In particular, we predict that the heat flow can be controlled by gating the emitter states. The gating of the states effectively allows to tune the Kondo temperature and the Kondo resonances. To observe the reported trends in actual measurements requires that either the source or the drain nanoparticles to be at thermal equilibrium, where the emitter states and the electron-phonon coupling can be tuned to demonstrate the strong effect of the electron-phonon coupling on heat flow. We are particularly excited for the prospect of the measurement to confirm the heat flow increase in the presence of the Kondo resonances at about $42T_K$ under the effect of phonon coupling. More specifically, the entropy current reduces to $I_s = (KA\Delta T)/(T - \Delta T)$.Here K is the thermal conductivity, A is the cross section of the junction and ΔT is the temperature gradient.

Declaration of competing interest

The authors declare that they have no known competing financial interests or personal relationships that could have appeared to influence the work reported in this paper.

Acknowledgements

A.G. grateful to the Tubitak for financial support via grant 114F195. B.D.D. acknowledges support by DOE, Basic Energy Science under Award DE-SC0016501.

APPENDIX

Green functions and Dyson equations

In this Appendix, we define the Green functions and then present the detailed structure of the Dyson equations for these Green functions. We also outline the numerical procedure employed to solve the Dyson equations.

The lesser Green functions can be defined in connection with the operators introduced in the main text as $\overline{G}^{<}_{g(e)}(t,t') = G^{<}_{g(e)}(t,t')e^{\varphi(t-t')} = < f^{\dagger}_{g(e)\sigma}(t')f_{g(e)\sigma}(t) > e^{\varphi(t-t')}$ and $B^{<}_{g(e)}(t,t') = < b^{\dagger}_{g(e)}(t')b_{g(e)}(t) >$ while the greater ones are $\overline{G}^{>}_{g(e)}(t,t') = G^{>}_{g(e)}(t,t')e^{\varphi(t'-t)} = < f_{g(e)\sigma}(t)f^{\dagger}_{g(e)\sigma}(t') > e^{\varphi(t'-t)}$ and $B^{>}_{g(e)}(t,t') = < b_{g(e)}(t)b^{\dagger}_{g(e)}(t') >$. In these expressions, phase factors defined as $\varphi(t-t') = \log_e < X^{\dagger}(t')X(t) >$ turn out to be [43].

$$\begin{aligned}\varphi(t-t') &= -V_{e-p}N_{ph}(1-e^{-i\omega_0(t-t')}) - \\ &\quad V_{e-p}(N_{ph}+1)(1-e^{i\omega_0(t-t')}),\end{aligned} \tag{A-1}$$

where $V_{e-p} = \lambda^2/\omega_0^2$. The combination of these analytic pieces yields the retarded functions such that

$$\begin{aligned}G^{r}_{g(e)}(t,t') &= -i\theta(t-t')[G^{>}_{g(e)}(t,t')e^{\varphi(t'-t)} + \\ &\quad G^{<}_{g(e)}(t,t')e^{\varphi(t-t')}] \\ B^{r}_{g(e)}(t,t') &= -i\theta(t-t')[B^{>}_{g(e)}(t,t') - B^{<}_{g(e)}(t,t')].\end{aligned} \tag{A-2}$$

These are the strict mathematical definitions of a retarded Green function before imposing any physical constraint such as the projection into $Q_B = 1$ subspace and they are identical to Eq. (6) in another study by Aguado et al. [60] for $\varphi = 0$. The projection into $Q_B = 1$ subspace is performed after the Green functions are inserted into the Dyson equations in our procedure. Therefore, both sides of the Dyson equations have the same Q_B dependency which ensures a fully consistent treatment of this problem as explained below.

Electron-electron interactions typically overwhelm the plasmon-exciton coupling within the quantum emitter as a result of the quantum confinement. Consequently, the plasmon-exciton coupling can be considered as a perturbation and the Dyson equations for the Green functions defined above can be constructed as

$$\begin{aligned}&\left(i\frac{\partial}{\partial t} - \epsilon_{g(e)}\right)G^{r}_{g(e)}(t,t') = \delta(t-t') + \\ &\int_{-\infty}^{\infty} dt_1 \Sigma^{r}_{g(e)}(t,t_1)G^{r}_{g(e)}(t_1,t')\end{aligned} \tag{A-3}$$

$$i\frac{\partial}{\partial t}B^r_{g(e)}(t,t^{'}) = \delta(t-t^{'}) + \int_{-\infty}^{\infty} dt_1 \Pi^r_{g(e)}(t,t_1) B^r_{g(e)}(t_1,t^{'}) \tag{A-4}$$

$$\left(i\frac{\partial}{\partial t} - \epsilon_{g(e)}\right) G^<_{g(e)}(t,t^{'}) e^{\varphi(t-t^{'})} = \int_{-\infty}^{\infty} dt_1 \Sigma^r_{g(e)}(t,t_1) G^<_{g(e)}(t_1,t^{'}) e^{\varphi(t_1-t^{'})} + \int_{-\infty}^{\infty} dt_1 \Sigma^<_{g(e)}(t,t_1) G^a_{g(e)}(t_1,t^{'}) \tag{A-5}$$

$$i\frac{\partial}{\partial t}B^<_{g(e)}(t,t^{'}) = \int_{-\infty}^{\infty} dt_1 \Pi^r_{g(e)}(t,t_1) B^<_{g(e)}(t_1,t^{'}) + \int_{-\infty}^{\infty} dt_1 \Pi^<_{g(e)}(t,t_1) B^a_{g(e)}(t_1,t^{'}). \tag{A-6}$$

We now introduce the shorthand notation for the retarded Green functions such that

$$\begin{aligned} G^r_{g(e)}(t,t^{'}) &= -i\theta(t-t^{'})[G^>_{g(e)}(t,t^{'}) e^{\varphi(t^{'}-t)} + \\ G^<_{g(e)}(t,t^{'}) e^{\varphi(t-t^{'})}] &:= -i\theta(t-t^{'}) g_{g(e)}(t,t^{'}), \\ B^r_{g(e)}(t,t^{'}) &= -i\theta(t-t^{'})[B^>_{g(e)}(t,t^{'}) - B^<_{g(e)}(t,t^{'})] \\ &:= -i\theta(t-t^{'}) b_{g(e)}(t,t^{'}). \end{aligned} \tag{A-7}$$

The Dyson equations needed to calculate the retarded pseudofermion Green functions can be explicitly written as

$$\begin{aligned} \left(\frac{\partial}{\partial t} + i\epsilon_g\right) g_g(t,t^{'}) = &- \int_{t^{'}}^{t} dt_1 K^>_L(t,t_1) \widetilde{b}_g(t,t_1) g_g(t_1,t^{'}) \\ &- \int_{t^{'}}^{t} dt_1 |\Delta|^2 \widetilde{g}_e(t,t_1) \widetilde{b}_g(t,t_1) \widetilde{B}^<_e(t_1,t) P^<_L(t_1,t) \times \\ &g_g(t_1,t^{'}) \end{aligned} \tag{A-8}$$

and

$$\begin{aligned} \left(\frac{\partial}{\partial t} + i\epsilon_e\right) g_e(t,t^{'}) = &- \int_{t^{'}}^{t} dt_1 K^>_R(t,t_1) \widetilde{b}_e(t,t_1) g_e(t_1,t^{'}) \\ &- \int_{t^{'}}^{t} dt_1 |\Delta|^2 \widetilde{g}_g(t,t_1) \widetilde{b}_e(t,t_1) \widetilde{B}^<_g(t_1,t) P^>_R(t,t_1) \times \\ &g_e(t_1,t^{'}) \end{aligned} \tag{A-9}$$

where the pseudofermion and slave-boson self energies and their projections into $Q_{B,g(e)} = 1$ have been obtained using the NCA procedure outlined earlier [37].Here, we have to mention that NCA captures dynamical quantities accurately at temperatures above $0.1T_K$ [45]. The Kernels $K^{>,<}_{L(R)}(t,t^{'})$ can be expressed in terms of the density of states of the metal nanoparticles $\rho(\epsilon)$ with a half bandwidth of D as

$$\begin{aligned} K^<_{L(R)}(t,t^{'}) &= \overline{\Gamma} \int_{-D}^{D} \frac{d\epsilon}{2\pi} \rho(\epsilon) \frac{1}{1+e^{\beta_{L(R)}\epsilon}} e^{i\epsilon(t-t^{'})} \\ K^>_{L(R)}(t,t^{'}) &= \overline{\Gamma} \int_{-D}^{D} \frac{d\epsilon}{2\pi} \rho(\epsilon) \frac{e^{\beta_{L(R)}\epsilon}}{1+e^{\beta_{L(R)}\epsilon}} e^{i\epsilon(t-t^{'})}, \end{aligned} \tag{A-10}$$

where $\beta_{L(R)} = 1/T_{L(R)}$ and we assume

$$\begin{aligned} \overline{\Gamma} &= \overline{\Gamma}_{L,g} = 2\pi |V_{L,g}(\epsilon_f)|^2 \\ \overline{\Gamma} &= \overline{\Gamma}_{R,e} = 2\pi |V_{R,e}(\epsilon_f)|^2. \end{aligned} \tag{A-11}$$

In these expressions, the Fermi level of the metal nanoparticles is represented by ϵ_f. To reach these equations, tunneling terms are assumed to be time and energy independent such that $V_{K,g(e)}(\epsilon) = V_{K,g(e)}(\epsilon_f)$ and the coupling of each discrete level with the metal nanoparticles is taken to be equal, i.e. $V_{L,g} = V_{R,e}$ which leads to Eq. A-11. Furthermore, we suppose $\Gamma(\epsilon) = \overline{\Gamma}\rho(\epsilon)$ and $\Gamma = \overline{\Gamma}\rho(\epsilon_f)$.

The Dyson equations for the retarded slave boson Green functions can be set up similarly as

$$\begin{aligned}\frac{\partial}{\partial t}b_g(t,t') &= -\int_{t'}^{t} dt_1 K_L^<(t_1,t)\widetilde{g}_g(t,t_1)b_g(t_1,t') \\ &- \int_{t'}^{t} dt_1|\Delta|^2\widetilde{g}_g(t,t_1)\widetilde{b}_e(t,t_1)\widetilde{G}_e^<(t_1,t) \\ &\times e^{\varphi(t_1-t)}P_L^>(t,t_1)b_g(t_1,t') \\ &+ \int_{t'}^{t} dt_1|\Delta|^2\widetilde{g}_g(t,t_1)\widetilde{B}_e^<(t,t_1)\widetilde{g}_e(t_1,t) \\ &\times P_L^<(t,t_1)b_g(t_1,t') \\ &- \int_{t'}^{t} dt_1|\Delta|^2\widetilde{g}_g(t,t_1)\widetilde{B}_e^<(t,t_1)\widetilde{g}_e(t_1,t) \\ &\times P_L^>(t,t_1)b_g(t_1,t') \\ &+ \int_{t'}^{t} dt_1|\Delta|^2\widetilde{g}_g(t,t_1)\widetilde{B}_e^<(t,t_1)\widetilde{g}_e(t_1,t) \\ &\times (P_L^>(t,t_1)-P_L^<(t,t_1))b_g(t_1,t'). \end{aligned} \tag{A-12}$$

and

$$\begin{aligned}\frac{\partial}{\partial t}b_e(t,t') &= -\int_{t'}^{t} dt_1 K_R^<(t_1,t)\widetilde{g}_e(t,t_1)b_e(t_1,t') \\ &- \int_{t'}^{t} dt_1|\Delta|^2\widetilde{g}_e(t,t_1)\widetilde{b}_g(t,t_1)\widetilde{G}_g^<(t_1,t) \\ &\times e^{\varphi(t_1-t)}P_R^<(t_1,t)b_e(t_1,t') \\ &+ \int_{t'}^{t} dt_1|\Delta|^2\widetilde{g}_e(t,t_1)\widetilde{B}_g^<(t,t_1)\widetilde{g}_g(t_1,t) \\ &\times P_R^>(t_1,t)b_e(t_1,t') \\ &- \int_{t'}^{t} dt_1|\Delta|^2\widetilde{g}_e(t,t_1)\widetilde{B}_g^<(t,t_1)\widetilde{g}_g(t_1,t) \\ &\times P_R^<(t_1,t)b_e(t_1,t') \\ &- \int_{t'}^{t} dt_1|\Delta|^2\widetilde{g}_e(t,t_1)\widetilde{B}_g^<(t,t_1)\widetilde{g}_g(t_1,t) \\ &\times (P_R^>(t_1,t)-P_R^<(t_1,t))b_e(t_1,t'). \end{aligned} \tag{A-13}$$

In these equations, the Green functions with a tilde on top are calculated in the limit of vanishing plasmon-exciton coupling following the previous work [36–38]. It is important to stress that this is not an additional approximation. The projection into $Q_{B,g(e)} = 1$ simply enforces this decoupling procedure. Intuitively, it has to be performed because the plasmon-exciton coupling is already included in the Dyson equations by $|\Delta|^2$ factors and using Green functions with finite plasmon-exciton coupling would lead to double counting. Hence, our technique satisfies both the charge conservation and the Ward identities despite the fact that the plasmon-exciton coupling is treated to second order in single-particle Green functions.

The task then boils down to calculating the lesser Green functions after the retarded Green functions are obtained properly. The relevant Dyson equations for the pseudofermion lesser Green functions are

$$\begin{aligned}&\left(\frac{\partial}{\partial t}+i\epsilon_g\right)G_g^<(t,t')e^{\varphi(t-t')} = \\ &-\int_{-\infty}^{t} dt_1 K_L^>(t,t_1)\widetilde{b}_g(t,t_1)G_g^<(t_1,t')e^{\varphi(t_1-t')} \\ &-\int_{-\infty}^{t} dt_1|\Delta|^2\widetilde{g}_e(t,t_1)\widetilde{b}_g(t,t_1)\widetilde{B}_e^<(t_1,t) \\ &\times P_L^<(t_1,t)G_g^<(t_1,t')e^{\varphi(t_1-t')} \\ &+\int_{-\infty}^{t'} dt_1 K_L^<(t,t_1)\widetilde{B}_g^<(t,t_1)g_g(t_1,t') \\ &+\int_{-\infty}^{t'} dt_1|\Delta|^2G_e^<(t,t_1)e^{\varphi(t-t_1)}\widetilde{B}_g^<(t,t_1)\widetilde{b}_e(t_1,t) \\ &\times P_L^>(t_1,t)g_g(t_1,t') \end{aligned} \tag{A-14}$$

and

$$\begin{aligned}&\left(\frac{\partial}{\partial t}+i\epsilon_e\right)G_e^<(t,t')e^{\varphi(t-t')} = \\ &-\int_{-\infty}^{t} dt_1 K_R^>(t,t_1)\widetilde{b}_e(t,t_1)G_e^<(t_1,t')e^{\varphi(t_1-t')} \\ &-\int_{-\infty}^{t} dt_1|\Delta|^2\widetilde{g}_g(t,t_1)\widetilde{b}_e(t,t_1)\widetilde{B}_g^<(t_1,t)\end{aligned}$$

$$\times P_R^{>}(t,t_1)G_e^{<}(t_1,t')e^{\varphi(t_1-t')}$$
$$+\int_{-\infty}^{t'}dt_1 K_R^{<}(t,t_1)\widetilde{B}_e^{<}(t,t_1)g_e(t_1,t')$$
$$+\int_{-\infty}^{t'}dt_1|\Delta|^2\widetilde{G}_g^{<}(t,t_1)e^{\varphi(t-t_1)}\widetilde{B}_e^{<}(t,t_1)\widetilde{b}_g(t_1,t)$$
$$\times P_R^{<}(t,t_1)g_e(t_1,t') \tag{A-15}$$

while their counterparts for the slave boson lesser Green functions are

$$\begin{aligned}\frac{\partial}{\partial t}B_g^{<}(t,t') &= -\int_{-\infty}^{t}dt_1 K_L^{<}(t_1,t)\widetilde{g}_g(t,t_1)B_g^{<}(t_1,t')\\
&-\int_{-\infty}^{t}dt_1|\Delta|^2\widetilde{g}_g(t,t_1)\widetilde{b}_e(t,t_1)\widetilde{G}_e^{<}(t_1,t)\\
&\times e^{\varphi(t_1-t)}P_L^{>}(t,t_1)B_g^{<}(t_1,t')\\
&+\int_{-\infty}^{t}dt_1|\Delta|^2\widetilde{g}_g(t,t_1)\widetilde{B}_e^{<}(t,t_1)\widetilde{g}_e(t_1,t)\\
&\times P_L^{<}(t,t_1)B_g^{<}(t_1,t')\\
&-\int_{-\infty}^{t}dt_1|\Delta|^2\widetilde{g}_g(t,t_1)\widetilde{B}_e^{<}(t,t_1)\widetilde{g}_e(t_1,t)\\
&\times P_L^{>}(t,t_1)B_g^{<}(t_1,t')\\
&+\int_{-\infty}^{t}dt_1|\Delta|^2\widetilde{g}_g(t,t_1)\widetilde{B}_e^{<}(t,t_1)\widetilde{g}_e(t_1,t)\\
&\times(P_L^{>}(t,t_1)-P_L^{<}(t,t_1))B_g^{<}(t_1,t')\\
&+\int_{-\infty}^{t'}dt_1 K_L^{>}(t_1,t)\widetilde{G}_g^{<}(t,t_1)e^{\varphi(t-t_1)}b_g(t_1,t')\\
&+\int_{-\infty}^{t'}dt_1|\Delta|^2\widetilde{B}_e^{<}(t,t_1)\widetilde{G}_g^{<}(t,t_1)e^{\varphi(t-t_1)}\\
&\times\widetilde{g}_e(t_1,t)P_L^{<}(t,t_1)b_g(t_1,t')\end{aligned} \tag{A-16}$$

and

$$\begin{aligned}\frac{\partial}{\partial t}B_e^{<}(t,t') &= -\int_{-\infty}^{t}dt_1 K_R^{<}(t_1,t)\widetilde{g}_e(t,t_1)B_e^{<}(t_1,t')\\
&-\int_{-\infty}^{t}dt_1|\Delta|^2\widetilde{g}_e(t,t_1)\widetilde{b}_g(t,t_1)\widetilde{G}_g^{<}(t_1,t)\\
&\times e^{\varphi(t_1-t)}P_R^{<}(t_1,t)B_e^{<}(t_1,t')\\
&+\int_{-\infty}^{t}dt_1|\Delta|^2\widetilde{g}_e(t,t_1)\widetilde{B}_g^{<}(t,t_1)\widetilde{g}_g(t_1,t)\\
&\times P_R^{>}(t_1,t)B_e^{<}(t_1,t')\\
&-\int_{-\infty}^{t}dt_1|\Delta|^2\widetilde{g}_e(t,t_1)\widetilde{B}_g^{<}(t,t_1)\widetilde{g}_g(t_1,t)\\
&\times P_R^{<}(t_1,t)B_e^{<}(t_1,t')\\
&-\int_{-\infty}^{t}dt_1|\Delta|^2\widetilde{g}_e(t,t_1)\widetilde{B}_g^{<}(t,t_1)\widetilde{g}_g(t_1,t)\\
&\times(P_R^{>}(t_1,t)-P_R^{<}(t_1,t))B_e^{<}(t_1,t')\\
&+\int_{-\infty}^{t'}dt_1 K_R^{>}(t_1,t)\widetilde{G}_e^{<}(t,t_1)e^{\varphi(t-t_1)}b_e(t_1,t')\\
&+\int_{-\infty}^{t'}dt_1|\Delta|^2\widetilde{B}_g^{<}(t,t_1)\widetilde{G}_e^{<}(t,t_1)e^{\varphi(t-t_1)}\\
&\times\widetilde{g}_g(t_1,t)P_R^{>}(t_1,t)b_e(t_1,t').\end{aligned} \tag{A-17}$$

An important aspect regarding the structure of these equations is that the left and right plasmon Green functions are embedded into the Dyson equations above after they are determined using the previously reported procedure [36] where the temperature of each nanoparticle is encoded via the left and right Kernels $K_{L(R)}^{>,<}(t,t')$. The contribution to the entropy flux due to coupling to radiation field via plasmons is buried in the plasmon Green functions which are calculated separately for each metal nanoparticle due to the temperature gradient. Furthermore, we want to stress that it is imperative to keep the phase factors attached to the lesser pseudofermion Green functions throughout the calculations in order to describe the influence of the electron-phonon in an accurate way.

The plasmon-exciton coupling in this paper ranges between 20 and 60 meV following the work of Manjavacas et. all [42]. and hence it is two orders

of magnitude smaller than electron-electron interactions. Moreover, the laser irradiates only the metal nanoparticles as noted. Therefore, the only transition mechanism between the discrete states is via the plasmon-exciton coupling. This assumption enables us to decouple the 4 operator Green functions which correspond to the entire quantum emitter into 2 operator Green functions which represent each discrete state and treat the weak plasmon-exciton coupling as a perturbation.

Before we conclude, we would like to provide a brief outline of the method that is employed to solve the Dyson equations numerically. The first step in this method is to put them in a discretized form in a two dimensional cartesian grid whose axis values correspond to the time arguments of Green functions. In order to use the computer memory efficiently, the lower and upper triangular parts of a square matrix are used to store the values of the lesser and retarded green functions respectively. The main bottleneck in this type of problem is that the strong electron-electron interactions are captured by the tails along the sides away from the diagonal. As the ambient temperature starts to fall below the Kondo temperature, the decay of these tails gets gradually slower. Therefore, the convergence of the calculation is checked by increasing the matrix size for each temperature until the results no longer change. This usually requires having to use matrix sizes on the order of thousands for low temperatures. Furthermore, the size of the matrix for the plasmon Green functions has to be equal with the corresponding pseudofermion and slave boson ones as a consequence of this algorithm. Most of the technical details regarding the discretization and numerical implementation of the resulting set of equations have been presented previously and we refer the reader to these [45,46].

Data availability

The data that support the findings of this study are available from the corresponding author upon reasonable request.

Author statement

Ali Goker: Conceptualization, methodology, software and writing – original draft. Huseyin Aksu: Visualization, investigation, writing – review & editing. Barry D. Dunietz: Research analyis, discussion and manuscript review & editing.

References

[1] H.W. Kroto, J.R. Heath, S.C. O'Brien, S.C. Curl, R.E. Smalley, c_{60}: buckminsterfullerene, Nature 318 (1985) 162–163.
[2] W.Y. Kim, Y.C. Choi, S.K. Min, Y. Cho, K.S. Kim, Application of quantum chemistry to nanotechnology: electron and spin transport in molecular devices, Chem. Soc. Rev. 38 (2009) 2319–2333.
[3] N. J Tao, Electron transport in molecular junctions, in: Nanoscience and Technology: A Collection of Reviews from Nature Journals, World Scientific, 2010, pp. 185–193.
[4] S.V. Aradhya, L. Venkataraman, Single-molecule junctions beyond electronic transport, Nat. Nanotechnol. 8 (2013) 399–410.
[5] M.S. Tame, K.R. McEnery, S.K. Özdemir, J. Lee, S.A. Maier, M.S. Kim, Quantum plasmonics, Nat. Phys. 9 (2013) 329–340.
[6] S.A. Maier, P.G. Kik, H.A. Atwater, S. Meltzer, E. Harel, B.E. Koel, A.G. Requicha, Local detection of electromagnetic energy transport below the diffraction limit in metal nanoparticle plasmon waveguides, Nat. Mat. 2 (2003) 229–232.
[7] H.A. Atwater, A. Polman, Plasmonics for improved photovoltaic devices, Nat. Mater. 9 (2010) 205–213.
[8] K.R. Catchpole, A. Polman, Plasmonic solar cells, Optic Express 16 (2008) 21793–21800.
[9] J. Lee, A.O. Govorov, J. Dulka, N.A. Kotov, Bioconjugates of cdte nanowires and au nanoparticles: plasmon-exciton interactions, luminescence enhancement and collective effects, Nano Lett. 4 (2004) 2323–2330.
[10] S.V. Boriskina, H. Gasemi, G. Chen, Plasmonic materials for energy: from physics to applications, Mater. Today 16 (2013) 375–386.
[11] S.K. Cushing, N. Wu, Progress and perspectives of plasmon-enhanced solar energy conversion, J. Phys. Chem. Lett. 7 (2016) 666–675.
[12] J. Li, S.K. Cushing, F. Meng, T.R. Senty, A.D. Bristow, N. Wu, Plasmon-induced resonance energy transfer for solar energy conversion, Nat. Photon. 9 (2015) 601–607.
[13] C. Sönnichsen, T. Franzl, T. Wilk, G. von Plessen, J. Feldmann, Drastic reduction of plasmon damping in gold nanorods, Phys. Rev. Lett. 88 (2002), 077402.
[14] T.K. Hakala, A.J. Moilanen, A.I. Väkeväinen, R. Guo, J.P. Martikainen, K. S. Daskalakis, H.T. Rekola, A. Julku, P. Törmä, Bose-einstein condensation in a plasmonic lattice, Nat. Phys. 14 (2018) 739–744.
[15] J. Lykkebo, G. Romano, A. Gagliardi, A. Pecchia, G.C. Solomon, Single-molecule electronics: cooling individual vibrational modes by the tunneling current, J. Chem. Phys. 144 (2016) 114310.
[16] R. Moghaddasi Fereidani, D. Segal, Phononic heat transport in molecular junctions: quantum effects and vibrational mismatch, J. Chem. Phys. 150 (2019), 024105.
[17] H. Park, J. Park, A.K.L. Lim, E.H. Anderson, A.P. Alivisatos, P.L. McEuen, Nanomechanical oscillations in a single-c60 transistor, Nature 407 (2000) 57–60.
[18] N.B. Zhitenev, H. Meng, Z. Bao, Conductance of small molecular junctions, Phys. Rev. Lett. 88 (2002) 226801–226805.
[19] B.J. LeRoy, S.G. Lemay, J. Kong, C. Dekker, Electrical generation and absorption of phonons in carbon nanotubes, Nature 432 (2004) 371–374.
[20] L.H. Yu, D. Natelson, The kondo effect in c60 single-molecule transistors, Nano Lett. 4 (2004) 79–83.
[21] K.J. Franke, J. Ignacio Pascual, Effects of electron–vibration coupling in transport through single molecules, J. Phys. Condens. Matter 24 (2012) 394002–394016.
[22] S.-I. Tanaka, M. Matsunami, S.-I. Kimura, An investigation of electron-phonon coupling via phonon dispersion measurements in graphite using angle-resolved photoelectron spectroscopy, Sci. Rep. 3 (2013) 3031–3035.
[23] T. Meier, F. Menges, P. Nirmalraj, H. Hölscher, H. Riel, B. Gotsmann, Length-dependent thermal transport along molecular chains, Phys. Rev. Lett. 113 (2014), 060801–060805.
[24] N. Sergueev, S. Seungha, M. Kaviany, B.D. Dunietz, Efficiency of thermoelectric energy conversion in biphenyl-dithiol junction: the effect of electron-phonon interaction, Phys. Rev. B 83 (2011) 195415.
[25] D. Bitan, M. Bhaskaran, Non-linear phonon peltier effect in dissipative quantum dot systems, Sci. Rep. 8 (2018) 5185.
[26] S. Hatef, S. Sara, L.J. Colin, Oligoyne molecular junctions for efficient room temperature thermoelectric power generation, Nano Lett. 15 (2015) 7467–7472.
[27] J.A. Schuller, E.S. Barnard, W. Cai, Y.C. Jun, J.S. White, M.L. Brongersma, Plasmonics for extreme light concentration and manipulation, Nat. Mater. 9 (2010) 193–204.
[28] I. Grigorenko, Quantum theory for plasmon-assisted local field enhancement, Phys. E Low-dimens. Syst. Nanostruct. 75 (2016) 302–308.
[29] G.A. Wurtz, P.R. Evans, W. Hendren, R. Atkinson, W. Dickson, R.J. Pollard, A. V. Zayats, W. Harrison, C. Bower, Molecular plasmonics with tunable exciton-plasmon coupling strength in j-aggregate hybridized au nanorod assemblies, Nano Lett. 7 (2007) 1297–1303.
[30] M. Ramezani, A. Halpin, A.I. Fernandez-Dominguez, J. Feist, S.R.K. Rodriguez, F. J. Garcia-Vidal, J. Gomez-Rivas, Plasmon-exciton-polariton lasing, Optica 4 (2017) 31–37.
[31] J. Galego, F.J. Garcia-Vidal, J. Feist, Suppressing photochemical reactions with quantized light fields, Nat. Commun. 7 (1–6) (2016) 13841.
[32] R.Q. Li, F.J. Garcia-Vidal, A.I. Fernandez-Dominguez, Plasmon-exciton coupling in symmetry-broken nanocavities, ACS Photonics 5 (2018) 177–185.
[33] D.E. Gomez, H. Giessen, T.J. Davis, Semiclassical plexcitonics: simple approach for designing plexcitonic nanoparticles, J. Phys. Chem. C 118 (2014) 23963–23969.
[34] A. Fihey, F. Maurel, A. Perrier, Plasmon-excitation coupling for dithienylethene/gold nanoparticle hybrid systems: a theoretical study, J. Phys. Chem. C 119 (2015) 9995–10006.
[35] A. Delga, J. Feist, J. Bravo-Abad, F.J. Garcia-Vidal, Theory of strong coupling between quantum emitters and localized surface plasmons, J. Optic. 16 (1–8) (2014) 114018.
[36] A. Goker, Strongly correlated plexcitonics: evolution of the fano resonance in the presence of kondo correlations, Phys. Chem. Chem. Phys. 17 (2015) 11569–11576.
[37] A. Goker, H. Aksu, Quantum transport through a coulomb blockaded quantum emitter coupled to a plasmonic dimer, Phys. Chem. Chem. Phys. 18 (2016) 1980–1991.
[38] A. Goker, Entropy current through a strongly correlated plexcitonic nanojunction, J. Phys. Chem. C 122 (2018) 4607–4614.
[39] I.G. Lang, Y.A. Firsov, Kinetic theory of semiconductors with low mobility, Sov. Phys. JETP 16 (1963) 1301–1312.
[40] Z.Z. Chen, R. Lu, B.F. Zhu, Effects of electron-phonon interaction on nonequilibrium transport through a single-molecule transistor, Phys. Rev. B 71 (2005) 165324.
[41] A.C. Hewson, D.M. Newns, On the local polaron model and its applications to intermediate valence systems, J. Phys. C Solid State Phys. 13 (1980) 4477–4494.
[42] A. Manjavacas, F.J. Garcia de Abajo, P. Nordlander, Quantum plexcitonics: strongly interacting plasmons and excitons, Nano Lett. 11 (2011) 2318–2323.

[43] A. Goker, Transient electron dynamics in a vibrating quantum dot in the kondo regime, J. Phys. Condens. Matter 23 (2011) 125302–125308.
[44] P. Nordlander, M. Pustilnik, Y. Meir, N.S. Wingreen, D.C. Langreth, How long does it take for the kondo effect to develop? Phys. Rev. Lett. 83 (1999) 808–811.
[45] H.X. Shao, D.C. Langreth, P. Nordlander, Many-body theory for charge-transfer in atom-surface collisions, Phys. Rev. B 49 (1994) 13929–13947.
[46] A.F. Izmaylov, A. Goker, B.A. Friedman, P. Nordlander, Transient currents in a quantum dot subject to a changer in coupling to its leads, J. Phys. Condens. Matter 18 (2006) 8995–9006.
[47] J. Kondo, Resistance minimum in dilute magnetic alloys, Prog. Theor. Phys. 32 (1964) 37–49.
[48] N.E. Bickers, D.L. Cox, J.W. Wilkins, Self-consistent large-*n* expansion for normal-state properties of dilute magnetic alloys, Phys. Rev. B 36 (1987) 2036–2079.
[49] P. Roura-Bas, L. Tosi, A.A. Aligia, K. Hallberg, Interplay between quantum interference and kondo effects in nonequilibrium transport through nanoscopic systems, Phys. Rev. B 84 (2011), 073406.
[50] A.C. Hewson, D. Meyer, Numerical renormalization group study of the anderson-holstein impurity model, J. Phys. Condens. Matter 14 (2001) 427–445.
[51] R.C. Monreal, A. Martin-Rodero, Equation of motion approach to the anderson-holstein Hamiltonian, Phys. Rev. B 79 (2009) 115140.
[52] P. Roura-Bas, L. Tosi, A.A. Aligia, Nonequilibrium transport through magnetic vibrating molecules, Phys. Rev. B 87 (2013) 195136.
[53] P. Roura-Bas, F. Güller, L. Tosi, A.A. Aligia, "Destructive quantum interference in transport through molecules with electron–electron and electron-vibration interactions, J. Phys. Condens. Matter 31 (2019) 465602.
[54] M. Plihal, D.C. Langreth, P. Nordlander, Transient currents and universal timescales for a fully time-dependent quantum dot in the kondo regime, Phys. Rev. B 71 (2005) 165321.
[55] P. Coleman, Phys. Rev. B 29 (1984) 3035.
[56] N.E. Bickers, Review of techniques in the large-n expansion for dilute magnetic alloys, Rev. Mod. Phys. 59 (1987) 845.
[57] L. Cui, W. Jeong, S. Hur, M. Matt, J.C. Klöckner, F. Pauly, P. Nielaba, J.C. Cuevas, E. Meyhofer, P. Reddy, Quantized thermal transport in single-atom junctions, Science 355 (2017) 1192–1195.
[58] L. Cui, S. Hur1, Z. Alaia A, J.C. Klïckner, W. Jeong, F. Pauly, S.-Y. Jang, P. Reddy, E. Meyhofer, Thermal conductance of single-molecule junctions, Nature 572 (2019) 628–633.
[59] K.H. Yang, Y.L. Zhao, Y.J. Wu, Y.P. Wu, Phonon-assisted thermoelectric effects in strongly interacting quantum dot, Phys. Lett. 374 (2010) 2874.
[60] R. Aguado, D.C. Langreth, Kondo effect in coupled quantum dots: a noncrossing approximation, Phys. Rev. B 67 (2003) 245307.